# Estimation of pore pressure and phase transitions of water confined in nanopores with non-local density functional theory

Christelle Miqueu, David Grégoire

Accepted manuscript in Molecular Physics. DOI: 10.1080/00268976.2020.1742935
The final publication is available at: https://dx.doi.org/10.1080/00268976.2020.1742935

# Estimation of pore pressure and phase transitions of water confined in nanopores with Non-Local Density Functional Theory

Christelle Miqueu* and David Grégoire

*Univ Pau & Pays Adour / E2S UPPA, Laboratoire des Fluides Complexes et leurs Réservoirs – IPRA, UMR5150, 64600, Anglet, France.*

*Christelle Miqueu : christelle.miqueu@univ-pau.fr

ORCID-ID : C. Miqueu : 0000-0002-0924-4437
D. Grégoire : 0000-0003-4313-460X

# Pore pressure and phase transitions of water confined in nanopores with Non-Local Density Functional Theory

In this paper, the non-local density functional theory is used in combination with SAFT-VR, to investigate the pore pressure behaviour of water confined in various nanopores. Due to the efficiency and low computational cost of the method, many configurations and thermodynamic conditions are explored. In particular, capillary condensation and evaporation of water, their impact on the pore pressure, and the effect of surface activation are evaluated. Successive first-order phase transitions of ultra-confined water monolayer are also highlighted.

Keywords: density functional theory; SAFT-VR; adsorption; phase transitions ; nanopores ; confinement.



## 1. Introduction

The static and dynamic physical properties of confined water are significantly different from their equivalent in bulk phase [1]. As an example, novel phases of ice have been discovered recently in carbon nanotubes by Koga and coworkers [2,3] and in other structures such as graphene slit pores [4]. Han *et al.* [5] have shown that water may freeze by means of both first-order and continuous phase transitions in hydrophobic nanopores. Ruiz-Barragan *et al.* [4] have already noticed the peculiar behaviour of highly confined water and found that its properties drastically change at the level of both H-bonding and electronic structure thanks to ab initio molecular dynamics simulations. In a recent review dedicated to the molecular simulation studies of water confined in slit geometries, Zangi [6] have summarized the major part of the recent works showing that, in that case, water stratifies into layers and exhibits an oscillatory stress response according to pore size. More recently, Bampoulis *et al.* [1] have reviewed the current knowledge of the structure and the dynamics of water in many confinement situations. It has thus been evidenced

that water behaviour is extremely sensitive to the specific confinement conditions. The major part of the current knowledge about confined water has been obtained from simulations (molecular dynamics, *ab initio* and molecular simulations) [3–5, 7–11] and from some experiments [12–15]. In this paper, we propose an alternative approach by using a molecular density functional theory (DFT). Indeed, it has already been demonstrated that non-local DFT could be as accurate as molecular simulations to estimate the thermodynamic properties of confined model or real fluids [16–21] but with two interesting key features: i) a much lower computational cost enabling to explore many configurations, ii) a continuum framework that could be coupled with other continuum theories, as for instance poromechanics to understand the effect of adsorption on macroscopic deformation of porous materials. The efficiency of DFT in modelling confined real fluids is controlled on the one hand by the non-local treatment of the repulsive and short-range interactions. To that extent, the Modified Fundamental Measure Theory [11,12], whose superiority over other treatments is unanimous, is used in the present study. On the other hand, DFT must be based on an efficient description of the bulk equilibrium properties and thus on the governing molecular interactions of the considered fluid. To do so for water, NLDFT is used in this work in combination with the SAFT framework with the original parametrization proposed by Clark *et al.* [24] for water. The efficiency of the proposed NLDFT/SAFT-VR coupling in predicting confined water density has already been assessed in a previous work [25] by comparison with molecular simulations performed with the same water molecular model. The principal objective of this study is to pursue the analysis of confined water with this thermodynamic model by investigating the pore pressure behaviour of water confined in various nanopores. Even if NLDFT is now widely used for simple fluids and especially for the characterization of porous materials [26–28], its application to water – or at least to hard

associating fluids [29–34] – is scarce because the inhomogeneous free energy related to hydrogen bonding is far from easy to build. Solely very recently, Trejos *et al.* [35] have used DFT to study the solvation force of water-like fluids in slit-like pores, which is the only work related to the pore pressure induced by adsorption of water within a DFT framework. The SAFT/DFT used by Trejos and his coworkers is similar to the one proposed here for the terms related to the hard-sphere contributions but are different for the attractive ones. They study the influence of parameters such as the range of the square-well potential or the gas-solid potential depth on the solvation force, in the case of supercritical water or liquid water at room temperature. Here, the application of DFT for the computation of water pore pressure is essentially focused on subcritical water in order to focus on capillary phase transitions. The effect of surface activation is also analysed, which constitutes the other innovative point of this paper.

## 2. Theoretical Section

### *2.1. Brief overview of NLDFT-SAFT coupling for inhomogeneous water*

The principal equations concerning the version of the coupled NLDFT/SAFT-VR model used in this work to obtain the microstructure of confined water have been detailed elsewhere [25]. Therefore, the discussion on this theory will be limited to its most significant features.

In the DFT framework [7,8], the grand thermodynamic potential $\Omega$ of an inhomogeneous fluid in the presence of an external potential $V_{ext}$, in the grand canonical ensemble $(\mu, V, T)$ is assumed to be a functional of the molecular density $\rho(\vec{r})$ as

$$\Omega[\rho(\vec{r})] = \mathcal{F}[\rho(\vec{r})] + \int\{V_{ext}(\vec{r}) - \mu\}(\vec{r})d\vec{r} \quad (1)$$

where $\mathcal{F}[\rho(\vec{r})]$ is the Helmholtz free energy of the fluid.

The equilibrium density distribution is calculated through the minimization of the grand potential by solving the corresponding Euler-Lagrange equation

$$\frac{\delta\Omega[\rho(\vec{r})]}{\delta\rho(\vec{r})} = \frac{\delta\mathcal{F}[\rho(\vec{r})]}{\delta\rho(\vec{r})} + V_{ext}(\vec{r}) - \mu = 0 \quad (2)$$

As in the bulk SAFT-VR framework, water is considered as one sphere with four identical associating sites placed in a tetrahedral geometry [24]. In order to describe this inhomogeneous spherical associative monomer, the Helmholtz free energy functional is separated in the following contributions

$$\mathcal{F}[\rho(\vec{r})] = \mathcal{F}^{ideal}[\rho(\vec{r})] + \mathcal{F}^{HS}[\rho(\vec{r})] + \mathcal{F}_1^{sr}[\rho(\vec{r})] + \mathcal{F}_2[\rho(\vec{r})] + \mathcal{F}^{att}[\rho(\vec{r})] + \mathcal{F}^{assoc}[\rho(\vec{r})] \quad (3)$$

where $\mathcal{F}^{ideal}[\rho(\vec{r})]$ is the ideal free energy [17]. The interaction between monomers is described by [20]: (i) the hard-sphere contribution $\mathcal{F}^{HS}[\rho(\vec{r})]$ of the Modified Fundamental Measure Theory [11,12]; (ii) a Barker-Henderson high-temperature perturbation expansion treated in a mean-field approximation where $\mathcal{F}_1^{sr}[\rho(\vec{r})]$ is the first-order short-range contribution, $\mathcal{F}_2[\rho(\vec{r})]$ the second-order contribution and $\mathcal{F}^{att}[\rho(\vec{r})]$ the classical attractive term in the DFT formalism.

The associating functional $\mathcal{F}^{asso}[\rho(\vec{r})]$ is [6,13] :

$$\mathcal{F}^{asso}[\rho(\vec{r})] = 4k_BT \int d\vec{r} n_0(\vec{r})\zeta(\vec{r}) \left( lnX(\vec{r}) - \frac{X(\vec{r})}{2} + \frac{1}{2} \right) \quad (4)$$

where $n_0(\vec{r})$ is one of the weighted densities of the MFMT formalism, $\zeta(\vec{r})$ is a proportional factor proposed by Yu *et al.* [32] to extend the bulk association free energy to inhomogeneous system. $X(\vec{r})$ is the fraction of not-bonded sites as introduced in Wertheim's theory [14,15] and is computed as proposed by Malheiro *et al.* [25].

In order to apply the NLDFT formalism, the external potential $V_{ext}$ applied on the fluid must be specified. Here, water confined in slit-like pores is considered. Thus, the external potential applied to the fluid, due to the presence of the solid, is modeled by the "10-4-3" Steele's potential [39] from both surfaces separated by the distance $L$ :

$$V_{ext}(z) = V_{sf}(z) + V_{sf}(L - z) \tag{5}$$

with

$$V_{sf}(z) = 2\pi\rho_s\varepsilon_{sf}\sigma_{sf}^{\ 2}\Delta\left[\frac{2}{5}\left(\frac{\sigma_{sf}}{z}\right)^{10} - \left(\frac{\sigma_{sf}}{z}\right)^{4} - \frac{\sigma_{sf}^{\ 4}}{3\Delta\left(z + 0.61\Delta\right)^{3}}\right] \tag{6}$$

where $\rho_s$ is the density of the solid, $\Delta$ is the spacing between two parallel layers of the molecules constituting the solid, $\sigma_{sf}$ and $\varepsilon_{sf}$ are the interaction parameters determined by the Lorentz-Berthelot rules: $\sigma_{sf}=(\sigma_{ss}+\sigma_{ff})/2$ and $\varepsilon_{sf}=(\varepsilon_{ss}\varepsilon_{ff})^{1/2}$ where the subscript *ss* refers to the solid while the subscript *ff* refers to the fluid.

In order to mimic the case of a surface containing adsorption sites, an integrated potential can be added to the previous external potential, following the same philosophy that transforms the Lennard-Jones intermolecular potential to the Steele's one when integrated over the carbon planes. Thus, considering a virtual homogenous surface $S$ with a number of sites per area $\rho_{site}$ placed at a distance $z_{site}$ inside the pore, the potential $\phi^{HB}$ resulting from this surface is given by

$$\phi^{HB} = \int_S \rho_{site} U_{O-H}\, dS \tag{7}$$

This potential $\phi^{HB}$ is the same SW intermolecular potential that describes hydrogen bond between water molecules in the fluid:

$$U_{O-H} = \begin{cases} -\varepsilon_{HB} & if \quad r < \sigma_{HB} \\ 0 & otherwise \end{cases} \tag{8}$$

where we have defined $\sigma_{HB}$, from the site-site bonding volume $\kappa_{HB}$ of SAFT-VR [24], by

$$\sigma_{HB} = \left( \frac{3}{4\pi} \kappa_{HB} \right)^{1/3} \tag{9}$$

Integration of Equation (7) gives

$$\phi^{HB} = \begin{cases} -\pi \rho_S \varepsilon_{HB} [\sigma_{HB}^2 - (z - z_{site})^2] & if \ |z - z_{site}| < \sigma_{HB} \\ 0 & if \ |z - z_{site}| > \sigma_{HB} \end{cases} \tag{10}$$

### *2.2. Pore pressure from NLDFT formalism*

The pore pressure $\Pi_f$ can be obtained from the grand thermodynamic potential [40] as:

$$\Pi_f = -\frac{1}{A_0} \left( \frac{\partial \Omega}{\partial L} \right)_{T, A_0, \mu} \tag{11}$$

where $A_0$ is the surface of one wall constituting the pore.

In a previous work [41], we had demonstrated that in the case of a Steele-type external potential, the pore pressure becomes :

$$\Pi_f = -\int_0^L \rho(z) \frac{\partial V^{Steele}}{\partial z}(z) dz \tag{12}$$

Here, the extension to activated surfaces modelled with the potential defined in Equation (10) is proposed. The pore pressure is, in that case, made of two contributions as :

$$\Pi_f = -\int_0^L \rho(z) \frac{\partial V^{Steele}}{\partial z}(z) dz - 2\pi \varepsilon_{HB} \rho_S \int_0^L \rho(z) \, (z - z_{site}) dz \tag{13}$$

## 3. Results and Discussion

### *3.1. Pore pressure of water confined in graphitic micropores*

Let us first consider water confined between two parallel graphitic surfaces separated by a distance $L$ from carbon-center to carbon-center. The interaction parameters of the solid [42] are $\sigma_{ss}$ = 0.34 nm and $\varepsilon_{ss}/k_B$ = 28 K. The density of graphite is $\rho_s$ = 114 molecules/m$^3$ and the spacing between two parallel layers of graphite molecules constituting the wall is $\Delta$ = 0.335 nm. The water interaction parameters : $\sigma$ = 0.3303 nm, $\varepsilon/k_B$ = 300.43 K, $\lambda$ = 1.718, $\varepsilon_{HB}/k_B$ = 1336.9 K and $\kappa_{HB}$ = 0.89369 10$^{-3}$ nm$^3$ are the ones obtained by Clark *et al.* [24]. At thermodynamic conditions corresponding to bulk liquid water (*i.e.* here T = 425 K and P = 0.52 MPa), both the average density and pore pressure oscillate as a function of pore width for graphitic slit micropores as shown in Figure 1.

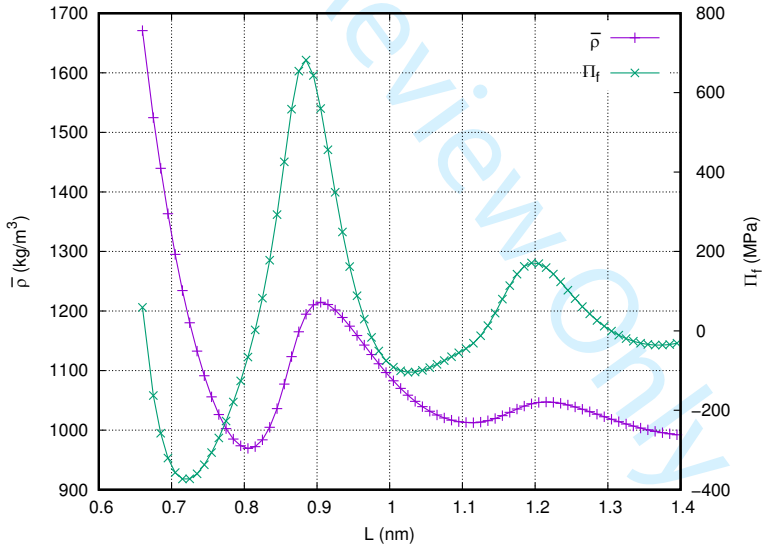


Figure 1. Average pore density and pore pressure as a function of pore size for water confined in slit graphitic pores at 425 K.

The global variation and oscillatory behaviour of the average density of water in slit micropores shown in Figure 1 is not surprising. It has already been described for other non-polar and polar fluids with molecular simulations [20, 21] and DFT calculations [36]. As a consequence of the layered structure, the pore pressure oscillates as a function of the distance between the solid walls with a periodicity approximately equal to the molecular diameter. It can be positive (effect of swelling due to repulsive forces) or negative (effect of shrinkage due to attractive forces) as a function of pore size; *i.e.* the fluid oscillates between alternative stable and instable configurations. The same behaviour has already been observed for supercritical methane with NLDFT calculation [41]. As summarised in Zangi's review [6], both experimental, molecular simulations and theoretical works have evidenced the oscillatory nature of the solvation forces of water confined between molecularly smooth surfaces. The NLDFT/SAFT-VR coupling is able to reproduce such an oscillatory behaviour with a period comparable to the one observed with transverse dynamic force microscopy [13].

### *3.2. Capillary condensation, hysteresis and their effect on pore pressure*

Interesting pore pressure behaviour can also be observed when capillary condensation occurs. As an example, Figure 2 depicts the capillary condensation and evaporation of water in a slit graphitic pore of width $L$ = 0.9 nm at 425 K, and the corresponding pore pressure behaviour. As seen in Figure 2, water average pore density increases with pressure upon adsorption until a capillary condensation due to confinement occurs at nearly half the saturation pressure. After this phase change, density of water saturated inside the pore continues increasing until bulk condensation at the bulk saturation pressure. The average density behaviour is monotonic and in agreement with molecular simulations. It can be well understood by looking at the density profiles plotted in Figure

3 for selected pressures. In all cases, the density profiles reveal the stratification of the confined water perpendicular to the graphitic walls. The stratified structure and the high densities of the water layers are consistent with results obtained with molecular dynamics simulations for water/graphene systems [4, 24].

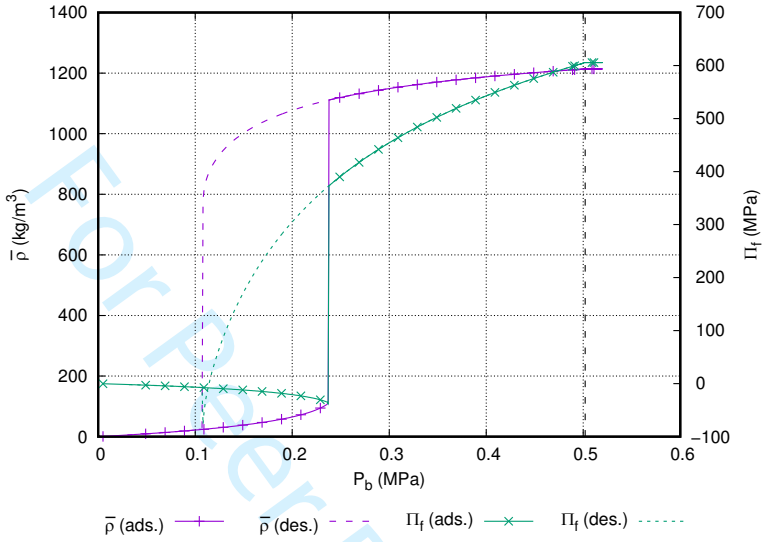


Figure 2. Average pore density and pore pressure as a function of bulk pressure for water confined in a slit graphitic pore of width 0.9 nm at 425 K. Solid lines: adsorption. Dashed lines: desorption. Vertical dotted line shows bulk saturation pressure.

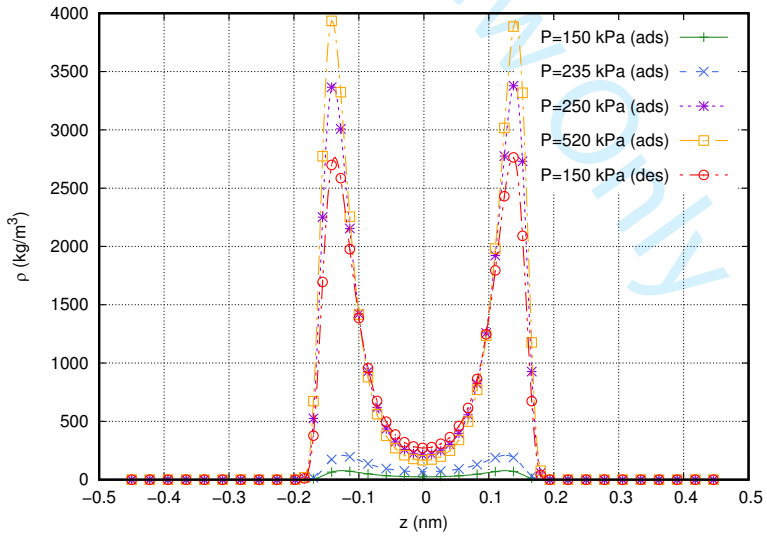


Figure 3. Water density profiles corresponding to some configurations of Fig 2.

Unlike the density, the pore pressure variation is different before and after the capillary phase transition, with negative decreasing values before condensation (suction effect on the solid), and positive increasing values after capillary condensation ("pushing" effect on the solid walls). This sudden change of pore pressure at condensation is interesting to be evaluated as its intensity is directly linked to the capillary forces that can deform the porous structure. The same analysis can also be performed during desorption. This time, density in the pore is decreasing with decreasing bulk pressure until capillary evaporation. This behaviour was already observed in a previous study [25]. The same kind of hysteresis is observed for pore pressure, in relation with pore density, but with a change in sign corresponding to the transition between repulsive and attractive configurations.

The computational low-cost of NLDFT/SAFT-VR coupling allows exploring many configurations. As observed in Figures 4a to 4d, detailed maps of density and pore pressure can be drawn. They allow to notice that the pore pressure behaviour is much more complex than the pore density one, passing from negative to positive values according to pore size, bulk pressure and adsorption or desorption. This leads us to say that, combined with water adsorption measurements, a measurable solvation pressure of water could be used as a good *probe* for pore size distribution determination.

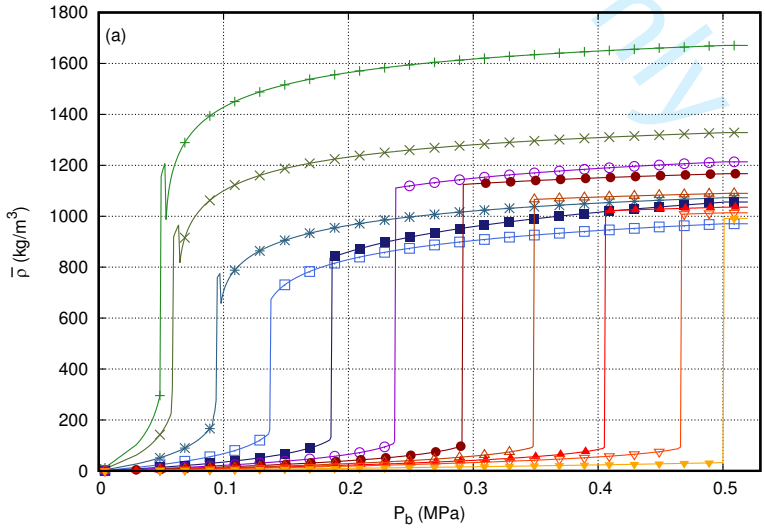

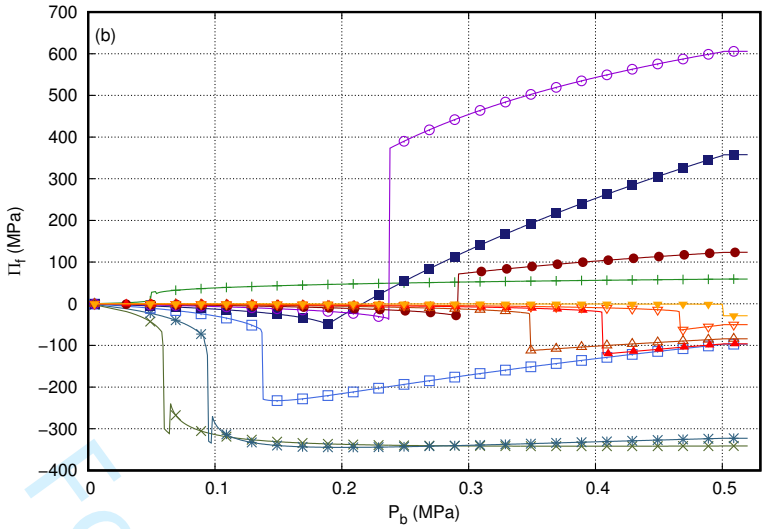


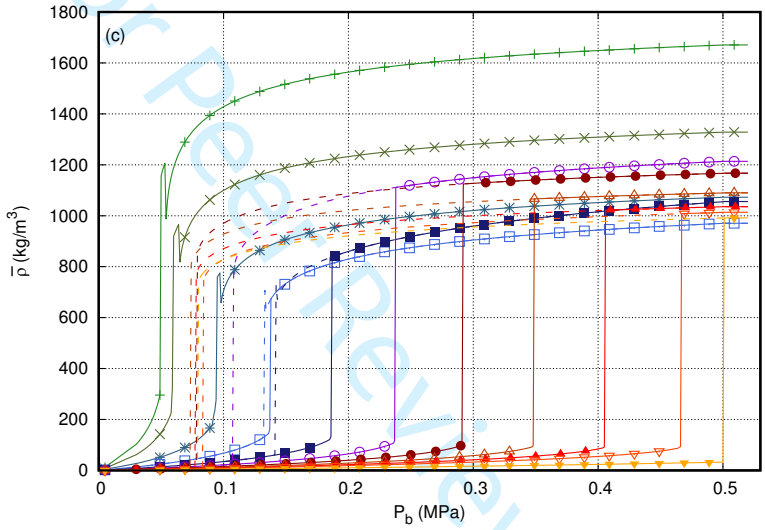


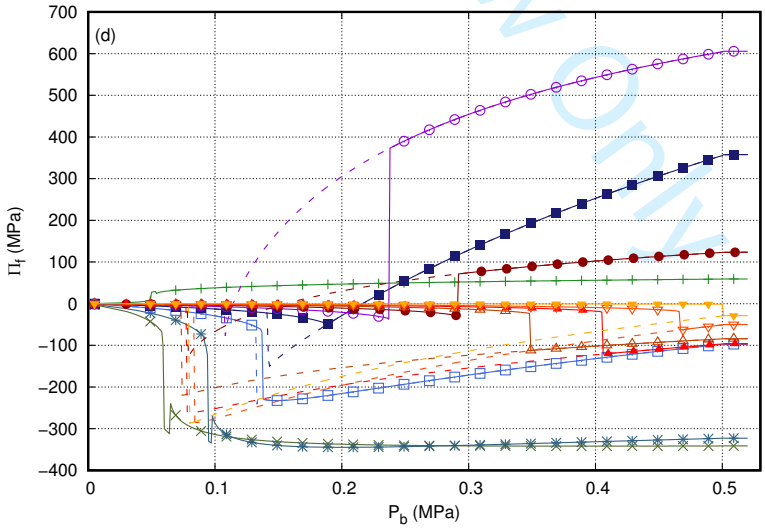


Figure 4. Adsorption: average pore density (a) and pore pressure (b) as a function of bulk pressure for water confined in slit graphitic micropores at 425 K. Adsorption + desorption for the same configurations (c & d): Solid lines: adsorption. Dashed lines: desorption.

### *3.3. Influence of surface activation on water pore pressure*

The ability of the NLDFT/SAFT-VR coupling used in this work to capture the adsorption of water in activated pores thanks to the modified external potential (see Equation (7)) has been demonstrated in a previous work [25]. Here, the effect of surface activation on pore pressure is illustrated in Figure 5 in a graphitic slit pore of width 1.4 nm, with and without activation sites. For this pore width, there is no capillary condensation for water when the surfaces correspond to pure graphite. The pore pressure is always negative as this pore size can accommodate two distinct layers of water whose global contribution is attractive. When the surfaces of the pore are doped with active sites (surface sites density of 2 $nm^{-2}$), capillary condensation occurs at 2.85 bar and is accompanied by an abrupt change in pressure sign leading to a repulsive configuration. This means that surface activation can have a drastic effect on water pore pressure and thus on the porous material deformation. Otherwise, this result shows that, if possible, pore pressure or swelling measurement could be used as an indirect measure of surface activation.

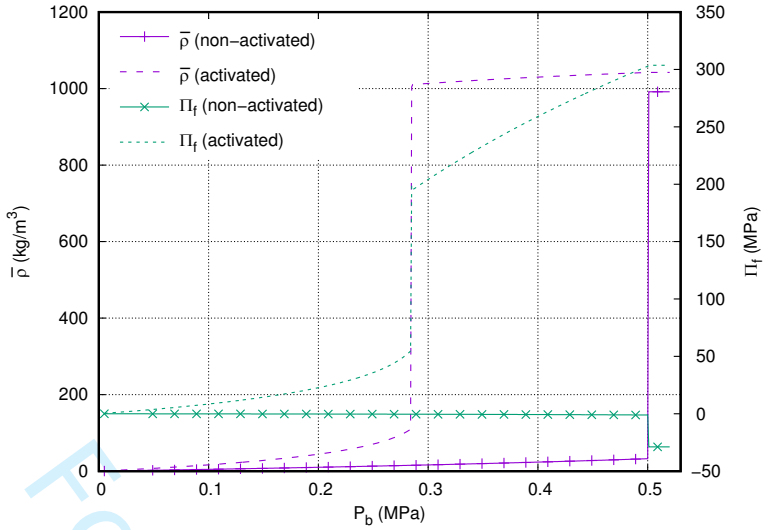


Figure 5. Average pore density (circles) and pore pressure (squares) as a function of bulk pressure for water confined in a slit micropore ($L$=1.4 nm) at 425 K. Solid lines: without activation. Dashed lines: with active sites (surface sites density of 2 nm$^{-2}$).

### *3.4. Successive capillary phase transitions*

NLDFT allows to explore in detail the global phase diagram of confined water with small pressure and temperature steps and find interesting behaviours that occur in tight P-T ranges. As an example, a part of the phase diagram of water confined in a slit-slit graphitic ultramicropore of width 0.66 nm, able to accommodate only one monolayer of water, is presented in Figure 6.

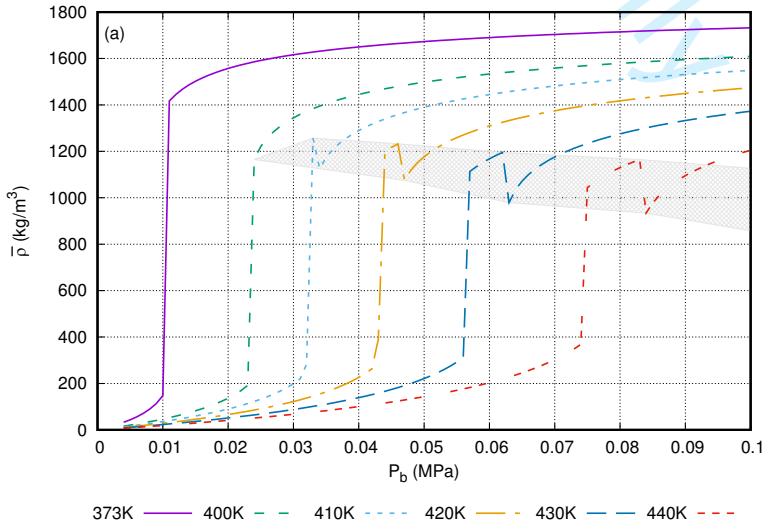

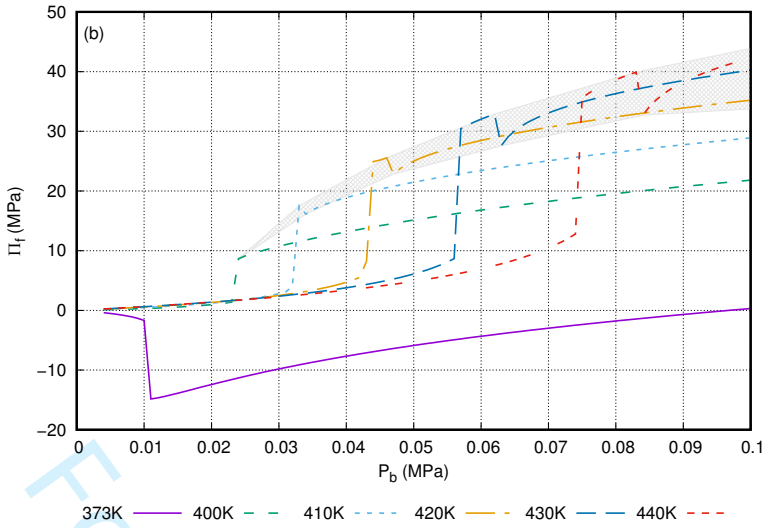


Figure 6. Average pore density (a) and pore pressure (b) as a function of bulk pressure for water confined in a slit graphitic micropore of width 0.66 nm for different temperatures.

One can see in this figure that ultra-confined water undergoes two successive first-order phase transitions for T > 400 K. The values of densities for the phase transitions are consistent with the phase diagram obtained by Han *et al.* [5] with MD simulations (TIP5P model for water). As NLDFT is a continuous formalism that does not allow access to the position of the molecules, it is difficult to know the *nature* of the intermediate phase obtained at these conditions. Indeed, the radial distribution function could be an efficient mean to distinguish between a solid-like or a liquid-like phase but here only one layer of water is accommodated within the pore and thus it is not possible to compute the long-ranged order that will enable us to distinguish between an ordered or a disordered phase. However, the calculation of the fraction of not-bonded sites $X$ that corresponds actually to the fraction of free hydrogen bonding in water can give some insights into the organisation of confined water. Before the first transition, approximately 80% of the HB sites of water are not-bonded, which is a typical value of a gas phase for bulk water [24]. After the second transition, this value is nearly 60 %, this time in agreement with bulk

liquid values [24]. The value for the intermediate phase (*i.e.* between the two transitions) is lower, corresponding to a degree of association of approximately 50 %, signing a more organised phase, such as an ice-like monolayer as already observed by several studies dedicated to the freezing of confined water. As an example, in a recent study, Agrawal *et al.* [7] have measured such freezing transition of water in carbon nanotubes at temperatures as high as 420 K with Raman spectroscopy. Klein and E. Kumacheva [46] observed with a surface force balance that the water monolayer undergoes an abrupt transition "to become solid-like" and Jinesh and Frenken [12] have observed with a high-resolution friction force microscope, at room temperature, that water confined between a tungsten tip and a graphite surface behaves like a solid. Mashl *et al.* [47] have shown with molecular dynamics simulations that water confined into carbon nanotubes under ambient conditions undergoes a transition into a state having an ice-like mobility. On the contrary, Zangi and Mark [8] have shown with molecular simulations that, for this confinement, water does not crystallize but forms a disordered liquid layer, which is also the conclusion of Bianco and Franzese [9] who observed a liquid-liquid phase transition ending in a critical point in the universality class of the two-dimensional Ising model.

To conclude with these capillary transitions, Brovchenko *et al.* [48] have made molecular simulations for TIP4P water confined in various hydrophobic pores. For a slit-like pore of 0.6 nm width, they have found a critical point at T = 402.5 ± 2.5 K, in perfect agreement with the value obtained here with the NLDFT/SAFT-VR model.

## Conclusions

In this paper, we have used the non-local density functional theory, in combination with the SAFT-VR, to compute the pore pressure of water in various nanopores. We have shown that NLDFT is a relevant and tractable tool to characterize confinement effects in that case as it allows computing many configurations (simple or activated surfaces) at

various thermodynamic conditions. It was shown that the pore pressure behavior of water in graphitic slit pores is much more complex than pore density, passing from negative to positive values according to pore size, bulk pressure and adsorption or desorption. This may have significant consequences at the macroscale such as volumetric swelling or shrinkage of nanoporous materials upon water adsorption/desorption. The capillary condensation and evaporation of water in nanopores and its impact on the pore pressure was also evaluated.

Finally, the NLDFT/SAFT-VR coupling has allowed to highlight successive first-order phase transitions of ultraconfined water monolayer, in agreement with recent experimental and simulations works.

## Disclosure statement

The authors reported no potential conflict of interest.

## Acknowledgements

D. Grégoire is fellow of the *Institut Universitaire de France*.

## References

[1] Bampoulis, P.; Sotthewes, K.; Dollekamp, E.; Poelsema, B. Water Confined in Two-Dimensions: Fundamentals and Applications. *Surf. Sci. Rep.*, **2018**, *73* (6), 233–264. https://doi.org/https://doi.org/10.1016/j.surfrep.2018.09.001.

[2] Takaiwa, D.; Hatano, I.; Koga, K.; Tanaka, H. Phase Diagram of Water in Carbon Nanotubes. *Proc. Natl. Acad. Sci.*, **2008**, *105* (1), 39 LP – 43. https://doi.org/10.1073/pnas.0707917105.

[3] Koga, K.; Gao, G. T.; Tanaka, H.; Zeng, X. C. Formation of Ordered Ice Nanotubes inside Carbon Nanotubes. *Nature*, **2001**, *412* (6849), 802–805. https://doi.org/10.1038/35090532.

[4] Ruiz-Barragan, S.; Muñoz-Santiburcio, D.; Marx, D. Nanoconfined Water within Graphene Slit Pores Adopts Distinct Confinement-Dependent Regimes. *J. Phys. Chem. Lett.*, **2019**, *10* (3), 329–334. https://doi.org/10.1021/acs.jpclett.8b03530.

[5] Han, S.; Choi, M. Y.; Kumar, P.; Stanley, H. E. Phase Transitions in Confined Water Nanofilms. *Nat. Phys.*, **2010**, *6*, 685.

[6] Zangi, R. Water Confined to a Slab Geometry: A Review of Recent Computer Simulation Studies. *J. Phys. Condens. Matter*, **2004**, *16* (45), S5371–S5388. https://doi.org/10.1088/0953-8984/16/45/005.

[7] Agrawal, K. V.; Shimizu, S.; Drahushuk, L. W.; Kilcoyne, D.; Strano, M. S. Observation of Extreme Phase Transition Temperatures of Water Confined inside Isolated Carbon Nanotubes. *Nat. Nanotechnol.*, **2016**, *12*, 267.

[8] Zangi, R.; Mark, A. E. Monolayer Ice. *Phys. Rev. Lett.*, **2003**, *91* (2), 25502. https://doi.org/10.1103/PhysRevLett.91.025502.

[9] Bianco, V.; Franzese, G. Critical Behavior of a Water Monolayer under Hydrophobic Confinement. *Sci. Rep.*, **2014**, *4*, 4440.

[10] Kolesnikov, A. I.; Loong, C.-K.; de Souza, N. R.; Burnham, C. J.; Moravsky, A. P. Anomalously Soft Dynamics of Water in Carbon Nanotubes. *Phys. B Condens. Matter*, **2006**, *385–386*, 272–274. https://doi.org/10.1016/J.PHYSB.2006.05.065.

[11] Koga, K.; Tanaka, H.; Zeng, X. C. First-Order Transition in Confined Water between High-Density Liquid and Low-Density Amorphous Phases. *Nature*, **2000**, *408* (6812), 564–567. https://doi.org/10.1038/35046035.

[12] Jinesh, K. B.; Frenken, J. W. M. Capillary Condensation in Atomic Scale Friction: How Water Acts like a Glue. *Phys. Rev. Lett.*, **2006**, *96* (16), 166103. https://doi.org/10.1103/PhysRevLett.96.166103.

[13] Antognozzi, M.; Humphris, A. D. L.; Miles, M. J. Observation of Molecular

Layering in a Confined Water Film and Study of the Layers Viscoelastic Properties. *Appl. Phys. Lett.*, **2001**, *78* (3), 300–302. https://doi.org/10.1063/1.1339997.

[14] Binggeli, M.; Mate, C. M. Influence of Capillary Condensation of Water on Nanotribology Studied by Force Microscopy. *Appl. Phys. Lett.*, **1994**, *65* (4), 415–417. https://doi.org/10.1063/1.113020.

[15] Choi, E.-M.; Yoon, Y.-H.; Lee, S.; Kang, H. Freezing Transition of Interfacial Water at Room Temperature under Electric Fields. *Phys. Rev. Lett.*, **2005**, *95* (8), 85701. https://doi.org/10.1103/PhysRevLett.95.085701.

[16] Davis, H. T. *Statistical Mechanics of Phases, Interfaces, and Thin Films*; VCH New York, 1996.

[17] Evans, R. Density Functionals in the Theory of Nonuniform Fluids. In *Fundamentals of Inhomogeneous Fluids*; Henderson, D., Ed.; Marcel Dekker Inc.: New York, NY, 1992; pp 85–176.

[18] Emborsky, C. P.; Feng, Z.; Cox, K. R.; Chapman, W. G. Recent Advances in Classical Density Functional Theory for Associating and Polyatomic Molecules. *Fluid Phase Equilib.*, **2011**, *306* (1), 15–30. https://doi.org/10.1016/j.fluid.2011.02.007.

[19] Dominik, A.; Tripathi, S.; Chapman, W. G. Bulk and Interfacial Properties of Polymers from Interfacial SAFT Density Functional Theory. *Ind. Eng. Chem. Res.*, **2006**, *45* (20), 6785–6792. https://doi.org/10.1021/ie060329e.

[20] Malheiro, C.; Mendiboure, B.; Plantier, F.; Blas, F. J.; Miqueu, C. Density Functional Theory for the Description of Spherical Non-Associating Monomers in Confined Media Using the SAFT-VR Equation of State and Weighted Density Approximations. *J. Chem. Phys.*, **2014**, *140* (13), 134707.

https://doi.org/10.1063/1.4869996.

[21] Bernet, T.; Piñeiro, M. M.; Plantier, F.; Miqueu, C. Effect of Structural Considerations on the Development of Free Energy Functionals for the Square-Well Fluid. *Mol. Phys.*, **2018**. https://doi.org/10.1080/00268976.2018.1438677.

[22] Hansen-Goos, H.; Roth, R. Density Functional Theory for Hard-Sphere Mixtures: The White Bear Version Mark II. *J. Phys. Condens. Matter*, **2006**, *18* (37), 8413–8425. https://doi.org/10.1088/0953-8984/18/37/002.

[23] Roth, R.; Evans, R.; Lang, a; Kahl, G. Fundamental Measure Theory for Hard-Sphere Mixtures Revisited: The White Bear Version. *J. Phys. Condens. Matter*, **2002**, *14* (46), 12063–12078. https://doi.org/10.1088/0953-8984/14/46/313.

[24] Clark, G. N. I.; Haslam, A. J.; Galindo, A.; Jackson, G. Developing Optimal Wertheim-like Models of Water for Use in Statistical Associating Fluid Theory (SAFT) and Related Approaches. *Mol. Phys.*, **2006**, *104* (22–24), 3561–3581. https://doi.org/10.1080/00268970601081475.

[25] Malheiro, C.; Mendiboure, B.; Míguez, J.-M. J.-M.; Piñeiro, M. M.; Miqueu, C. Nonlocal Density Functional Theory and Grand Canonical Monte Carlo Molecular Simulations of Water Adsorption in Confined Media. *J. Phys. Chem. C*, **2014**, *118* (43), 24905–24914. https://doi.org/10.1021/jp505239e.

[26] Lowell, S.; Shields, J. E.; Thomas, M. A.; Thommes, M. *Characterization of Porous Solids and Powders: Surface Area, Pore Size and Density*, Particle T.; Springer: Dordrecht, 2010.

[27] Neimark, A. V; Lin, Y.; Ravikovitch, P. I.; Thommes, M. Quenched Solid Density Functional Theory and Pore Size Analysis of Micro-Mesoporous Carbons. *Carbon N. Y.*, **2009**, *47* (7), 1617–1628.

[28] Jagiello, J.; Thommes, M. Comparison of DFT Characterization Methods Based

on N2, Ar, CO2, and H2 Adsorption Applied to Carbons with Various Pore Size Distributions. *Carbon N. Y.*, **2004**, *42* (7), 1227–1232. https://doi.org/10.1016/j.carbon.2004.01.022.

[29] Sokolowski, S.; Fischer, J. The Role of Attractive Intermolecular Forces in the Density Functional Theory of Inhomogeneous Fluids. **1992**, *96* (April), 5441–5447.

[30] Bymaster, A.; Dominik, A.; Chapman, W. G. Hydration Structure and Interfacial Properties of Water near a Hydrophobic Solute from a Fundamental Measure Density Functional Theory. *J. Phys. Chem. C*, **2007**, *111* (43), 15823–15831. https://doi.org/10.1021/jp073762q.

[31] Segura, C. J.; Chapman, W. G. Associating Fluids with Four Bonding Sites against Solid Surfaces: Monte Carlo Simulations. *Mol. Phys.*, **1995**, *86* (3), 415–442. https://doi.org/10.1080/00268979509413622.

[32] Yu, Y.-X.; Wu, J. A Fundamental-Measure Theory for Inhomogeneous Associating Fluids. *J. Chem. Phys.*, **2002**, *116* (16), 7094. https://doi.org/10.1063/1.1463435.

[33] Hughes, J.; Krebs, E. J.; Roundy, D. A Classical Density-Functional Theory for Describing Water Interfaces. *J. Chem. Phys.*, **2013**, *138* (2), 024509. https://doi.org/10.1063/1.4774155.

[34] Trejos, V. M.; Sokołowski, S.; Pizio, O. Adsorption and Phase Behavior of Water-like Fluid Models with Square-Well Attraction and Site-Site Association in Slit-like Pores: Density Functional Approach. *J. Chem. Phys.*, **2018**, *149* (13), 134701.

[35] Trejos, V. M.; Sokołowski, S.; Pizio, O. On the Solvation Force of Water-like Fluid Models with Square-Well Attraction and Site–Site Association in Slit-like

Pores: Density Functional Approach. *Mol. Phys.*, **2019**, 1–10.

[36] Davis, H. T. *Statistical Mechanics of Phases, Interfaces and Thin Films.*; Wiley-VCH: New-York, 1998.

[37] Wertheim, M. S. Fluids with Highly Directional Attractive Forces. I. Statistical Thermodynamics. *J. Stat. Phys.*, **1984**, *35* (1–2), 19–34.

[38] Wertheim, M. S. Fluids with Highly Directional Attractive Forces. III. Multiple Attraction Sites. *J. Stat. Phys.*, **1986**, *42* (3), 459–476. https://doi.org/10.1007/BF01127721.

[39] Steele, W. A. The Physical Interaction of Gases with Crystalline Solids. I. Gas-Solid Energies and Properties of Isolated Adsorbed Atoms. *Surf. Sci.*, **1973**, *36* (1), 317–352.

[40] Hansen, J.-P.; McDonald, I. R. *Theory of Simple Liquids*; 2006.

[41] Grégoire, D.; Malheiro, C.; Miqueu, C. Estimation of Adsorption-Induced Pore Pressure and Confinement in a Nanoscopic Slit Pore by a Density Functional Theory. *Contin. Mech. Thermodyn.*, **2017**. https://doi.org/10.1007/s00161-017-0602-x.

[42] Tan, Z.; Gubbins, K. E. Adsorption in Carbon Micropores at Supercritical Temperatures. *J. Phys. Chem.*, **1990**, *94* (15), 6061–6069.

[43] Diao, R.; Fan, C.; Do, D. D.; Nicholson, D. Monte Carlo Simulation of Adsorption-Induced Deformation in Finite Graphitic Slit Pores. *J. Phys. Chem. C*, **2016**, *120* (51), 29272–29282. https://doi.org/10.1021/acs.jpcc.6b10135.

[44] Do, D. D.; Nicholson, D.; Do, H. D. Effects of Adsorbent Deformation on the Adsorption of Gases in Slitlike Graphitic Pores: A Computer Simulation Study. *J. Phys. Chem. C*, **2008**, *112* (36), 14075–14089. https://doi.org/10.1021/jp8032269.

[45] Cicero, G.; Grossman, J. C.; Schwegler, E.; Gygi, F.; Galli, G. Water Confined in Nanotubes and between Graphene Sheets: A First Principle Study. *J. Am. Chem. Soc.*, **2008**, *130* (6), 1871–1878. https://doi.org/10.1021/ja074418+.

[46] Klein, J.; Kumacheva, E. Simple Liquids Confined to Molecularly Thin Layers. I. Confinement-Induced Liquid-to-Solid Phase Transitions. *J. Chem. Phys.*, **1998**, *108* (16), 6996–7009. https://doi.org/10.1063/1.476114.

[47] Mashl, R. J.; Joseph, S.; Aluru, N. R.; Jakobsson, E. Anomalously Immobilized Water: A New Water Phase Induced by Confinement in Nanotubes. *Nano Lett.*, **2003**, *3* (5), 589–592. https://doi.org/10.1021/nl0340226.

[48] Brovchenko, I.; Geiger, A.; Oleinikova, A. Water in Nanopores: II. The Liquid–Vapour Phase Transition near Hydrophobic Surfaces. *J. Phys. Condens. Matter*, **2004**, *16* (45), S5345–S5370. https://doi.org/10.1088/0953-8984/16/45/004.